NASA CONTRACTOR
REPORT

NASA CR-129036

M553 SPHERE FORMING EXPERIMENT
Pure Nickel Specimen Evaluation

By Philip C. Johnson and Edward T. Peters
Arthur D. Little, Inc.
Cambridge, Massachusetts

December 1973

Prepared for

NASA-GEORGE C. MARSHALL SPACE FLIGHT CENTER
Marshall Space Flight Center, Alabama 35812

TECHNICAL REPORT STANDARD TITLE PAGE

1. REPORT NO.	2. GOVERNMENT ACCESSION NO.	3. RECIPIENT'S CATALOG NO.
NASA CR-129036		

4. TITLE AND SUBTITLE	5. REPORT DATE
M553 Sphere Forming Experiment Pure Nickel Specimen Evaluation	December 1973
	6. PERFORMING ORGANIZATION CODE
7. AUTHOR(S) Philip C. Johnson and Edward T. Peters	8. PERFORMING ORGANIZATION REPORT #
9. PERFORMING ORGANIZATION NAME AND ADDRESS Arthur D. Little, Inc. Cambridge, Massachusetts	10. WORK UNIT NO.
	11. CONTRACT OR GRANT NO. NAS 8-28723
12. SPONSORING AGENCY NAME AND ADDRESS National Aeronautics and Space Administration Washington, D. C. 20546	13. TYPE OF REPORT & PERIOD COVERED Contractor Report
	14. SPONSORING AGENCY CODE

15. SUPPLEMENTARY NOTES

16. ABSTRACT

The only significant feature which was observed on the pure nickel flight specimens which differed significantly from the ground-based specimens is a region or cap of very fine two-dimensional surface growth structure at the top of the samples. This fine grain region was observed on three of the six samples evaluated. Such two-dimensional surface growth structures have been observed both on the ground-based specimens and on other surface areas of the flight specimens. However, the fine structures observed on the three flight samples are at least an order of magnitude finer than those previously observed, and resemble similar localized, fine, two-dimensional surface structures observed in both ground and flight specimens for the nickel alloys. The two-dimensional growth areas consist primarily of fine equiaxed grains in one specimen, SL-2.6, fine dendrites, SL-2.5, or a core of fine equiaxed grains surrounded by a ring of fine dendrites, Specimen SL-1.9.

17. KEY WORDS	18. DISTRIBUTION STATEMENT
	Unclassified - Unlimited L V K Vardaman

19. SECURITY CLASSIF. (of this report)	20. SECURITY CLASSIF. (of this page)	21. NO. OF PAGES	22. PRICE
Unclassified	Unclassified	45	NTIS

For sale by National Technical Information Service, Springfield, Virginia 22151

TABLE OF CONTENTS

PURE NICKEL SPECIMEN EVALUATION

SUMMARY

The only significant feature which was observed on the pure nickel flight specimens which differed significantly from the ground-based specimens is a region or cap of very fine two-dimensional surface growth structure at the top of the samples. This fine grain region was observed on three of the six samples evaluated. Such two-dimensional surface growth structures have been observed both on the ground-based specimens and on other surface areas of the flight specimens. However, the fine structures observed on the three flight samples are at least an order of magnitude finer than those previously observed, and resemble similar localized, fine, two-dimensional surface structures observed in both ground and flight specimens for the nickel alloys. The two-dimensional growth areas consist primarily of fine equiaxed grains in one specimen, SL-2.6, fine dendrites, SL-2.5, or a core of fine equiaxed grains surrounded by a ring of fine dendrites, Specimen SL-1.9.

A possible explanation for these structures is decreased bulk convection of the remnant liquid in the flight specimens as a result of the low gravity conditions. The flight specimen movie records show considerable turbulence or convection. It nevertheless may have been less than in the ground-based specimens. As the bulk of the specimens solidified, usually from the sting region and unmelted portions of the specimens, the latent heat of fusion released would not tend to distribute by means of bulk fluid flow as rapidly under conditions of relatively lower bulk fluid convection. This would tend to enhance the establishment of thermal conditions at the areas most remote from the advancing solid, such as the cap areas, which would favor independent two-dimensional nucleation and growth in these areas. There certainly are other factors involved, however, since not all of the pure nickel flight specimens exhibit this phenomenon. In the case of the slowly heated retained Specimen SL-2.2, this may be explained in terms of a relatively slow solidification rate. Thermal conduction of the latent heat through the remnant liquid would tend to negate favorable thermal conditions at areas remote from the growing solid even under conditions of minimized bulk fluid convection. The bulk of the specimens did not exhibit any solidification features which can be attributed to low gravity processing. There was no homogeneous nucleation or significant undercooling in the bulk. There may have been some slight undercooling in the areas of fine two-dimensional growth.

SAMPLE DISTRIBUTION

Six pure nickel specimens were evaluated. The catalogue numbers and principal contractors conducting the evaluations were:

SL-1.9	Georgia Institute of Technology
SL-1.10	University of Connecticut
SL-1.11	University of Connecticut
SL-2.2	Arthur D. Little, Inc.
SL-2.5	Georgia Institute of Technology
SL-2.6	Arthur D. Little, Inc.

The high purity nickel rod from which the specimens were prepared was supplied by the Materials Research Corporation as "VP Grade" vacuum processed, cold rolled, swaged and drawn in size. The chemical analysis as provided by the supplier is given in Table I.

TABLE I

VP Grade Nickel
Typical Emission Spectrographic Analysis

Element	Content (ppm)
C	50
O	20
N	<5
H	1
Fe	5
Si	5
S	< 10
Cu	< 15
Ti	10
Cr	2

LABORATORY STUDIES

I. EXPERIMENTAL METHODS

A. ARTHUR D. LITTLE, INC.

Visual Examination

In addition to the photographs supplied by MSFC, the samples were examined under a low power optical stereoscopic microscope. Aside from the general appearance of the samples, visual examination was used to identify areas for subsequent X-ray fluorescence, SEM topography, surface chemical analysis by energy-dispersive X ray, and optimum sectioning planes for metallography.

X-ray Fluorescence

The standard samples provided by T. Kattamis of the University of Connecticut were employed to provide calibration curves. The curves were linear over the range of concern. Analyses were conducted with a chromium target at 45kV-25ma, a LiF analyzing crystal and a scintillation detector. No attempt was made to analyze for lighter elements (i.e., $Z < 25$); therefore, their presence is not precluded. The major alloy element content was determined from the calibration curve. This analysis represents the average chemistry of a surface layer approximately 0.04 mm thick.

Density, Radiography and Unetched Cross Sections

These techniques have been grouped together, since they are all intended to determine the extent of porosity and its location within the sample. The density measurements were performed by MSFC and the data supplied to Arthur D. Little, Inc. Several of the densities are above theoretical, indicating the now generally recognized difficulties encountered in making accurate and useful density measurements. Density measurements made by Arthur D. Little, Inc., using the differential weight of the samples in air and water were equally inadequate, and are not reported here.

The radiographs were supplied by MSFC. Again, the spheres are difficult to radiograph, and the films are light (underexposed) and have low

contrast. Contact prints and 5X enlargements of the radiographs did not yield useful images. For the pure nickel samples, unetched cross sections proved most useful in determining porosity on a semiquantitative basis.

Sphericity

Sphericity data were provided to Arthur D. Little, Inc., by MSFC. These diameters were measured, on those specimens where possible, as viewed on the end or on a plane normal to the original sting axis (Z axis). We have also made shadowgraphs of the flight specimens both in the plane normal to the sting axis and on a plane through the Z axis (selected with reference to bulk geometrical or topographical features).

Pinhole Laue Diffraction Analysis

All of the specimens were examined in the as-received condition, utilizing a back reflection pinhole diffraction camera. Operating conditions were: copper tube, 35 kV, 20 ma, 5 minute exposure, 3 cm sample to film distance, 0.75 mm diameter collimator.

Energy Dispersive X-ray Analysis

The distribution of elements in the various specimens has been measured by means of an energy dispersive X-ray analyzer attachment to the scanning electron microscope. Due to the efficient stopping power of electrons by nickel, the analyses are limited to a surface layer approximately 3-4μm in depth. Analyses can be at a point (5 μm in diameter) or, by scanning the electron beam, averaged over a rather large area. Conversion of measured X-ray intensity to composition is accomplished by analyzing known chemistry standards. The results are semiquantitative due to some necessary simplifying assumptions, as follows:

1. The background correction for Ni, Ag, Cu and Sn peaks is based on appropriate measurements from the pure nickel standard.

2. The corrected data are normalized to nickel intensity to provide a common basis for comparison.

3. No correction can be easily made for the substantial variation in surface roughness of the various samples. As the standards had flat, metallographically polished surfaces, there can be a relative error of 10-20% in the sample results.

4. The Ni-Ag standards contained very low levels of silver (0.15 and 0.58 weight percent). The corresponding weak X-ray signal (and high background) led to considerable uncertainty in the calibration curve for the Ni-Ag system. The results for silver are therefore very qualitative.

In addition to collection of data for specific elements of interest, the data output reveals the presence of other contaminant elements. These of course are qualitative in nature. The analysis is completely nondestructive.

Metallography

The specimens were sectioned into roughly two halves using a silicon carbide slurry wire saw. This provides a very slow cool cut, with a kerf ranging from .1 to .2 mm. The section plane varied from each sample and was determined on the basis of prior nondestructive analyses for the purpose of maximizing the information which might be gained from the metallographic sections. One half of each specimen was mounted in transparent thermoplastic mounting material, mechanically polished successively through 240 to 600 grit papers, 6μm diamond on a beeswax lap, 1 μm diamond on the synthetic rayon nap cloth and .05 μm gamma alumina on a Syntron, again using a synthetic rayon nap cloth.

The pure nickel specimens were etched in Carapella's reagent to obtain the solidification structure, followed by Rosenhain's reagent to emphasize the recrystallization grain structure.

Microhardness

The microhardness of the sectioned specimens was measured on a Tukon microhardness tester. A Vickers indenter was used with a 500 gram load.

B. GEORGIA INSTITUTE OF TECHNOLOGY

Visual Observations

Each of the four Skylab specimens was carefully observed under a stereo microscope. Precise notes were taken concerning the shape of the specimens, the degree of melting, the presence of surface contaminants, and the position and nature of any unusual features.

Optical Macroscopy

Optical macrographs were taken of each of the specimens from six different orthogonal directions. These micrographs were taken on a Bausch & Lomb "L" camera using a 48 millimeter Micro Tessar lens. A few stereo-macrographs were recorded using a 6 degree tilt between the left and right views.

Radiography

Radiographs of each of the specimens were made using a Baltograph II X-ray generator operating at 135 KV with a tungsten target to reveal the position and size of any voids present.

Scanning Electron Microscopy

A Cambridge Stereoscan Mark II-A equipped with a Kevex-ray-Northern Scientific energy dispersive X-ray analyzer and a Quantimet 720 image analyzing computer was used to examine the Skylab specimens. Each of the specimens was mounted in a special stub designed to hold spheres and placed in the scanning electron microscope for observations. Micrographs of the surfaces were taken using the following systematic technique. Some great circle on the surface of each sample was chosen on which was exemplified all of the different surface features characteristic of that particular specimen. Low magnification micrographs (25X) were made in the SEM along that great circle at intervals of 30 degrees. Higher magnification micrographs were made in each area to show the typical surface structures, any unusual features, and any surface contaminants. The location of the area from which the higher magnification micrographs were made was marked on the low magnification shots. A few stereomicrographs were recorded using a 10 degree difference between the left and right views. Energy dispersive X-ray analysis for elemental content was performed on general areas of each specimen as well as on unusual features and contaminant particles.

Electron Probe Microanalysis

The electron probe microanalyzer was used for a more accurate analysis of the elemental content. Analyses were run in general areas of each specimen as well as on any unusual features found either through the optics of the microprobe or previously in the scanning electron microscope.

X-ray Fluorescence Spectroscopy

Quantitative elemental analysis of each sample on a gross scale was made using a Siemens Crystalloflex IV X-ray fluorescence unit operating at 40 KV with a tungsten target.

Section Preparations

Each of the specimens was positioned on a carbon block and held in place with sealing wax so that a cut could be made through a plane whose perimeter included all of the various structures seen on the specimen surface. Sectioning was done on a Micromatic Precision Wafering Maching using a .025 cm (10 mil) thick silicon carbide wheel. After sectioning, one half of each of the specimens was mounted in a casting resin so that the cut face could be prepared for examination. The specimens were mechanically polished using a series of abrasive papers and wet polishing wheels through a .3 μm alumina and electropolished using a Disa-Electropolisher. Electropolishing was accomplished on the pure Ni using the A2 electrolite solution containing:

Perchloric acid	$78 \times 10^{-6} m^3$
Distilled water	$120 \times 10^{-6} m^3$
Methyl alcohol	$700 \times 10^{-6} m^3$
Butyl cellosolve	$100 \times 10^{-6} m^3$

Emission Spectroscopy

A small amount of material was removed from the center of the unmounted half of each specimen by drilling a small shallow hole in the center of each cut face. The shavings thus produced were placed in a cavity of a carbon spectrographic rod and burned to completion in an Applied Research Laboratories 1.5 meter grating emission spectrograph. The near ultra violet radiation was recorded on Kodak Spectrum Analysis No. 1 Film and analyzed on an Applied Research Laboratories comparator.

Electron Probe Microanalysis of Sections

Each of the polished sections was analyzed in the electron microprobe. Analyses were made of general areas of the sections, across grains, in and along dendritic features, in eutectics and in any unusual features seen. Standards supplied by Dr. Theo Kattamis of the University of Connecticut were used to obtain quantitative data from these analyses.

Optical Examination of Specimen Sections

Optical macrographs of each of the polished and etched sections were taken using a Bausch and Lomb "L" camera and a 48 millimeter lens. Micrographs were taken to demonstrate all of the various microstructures present on each section using a Leitz Metallux optical microscope.

Scanning Electron Microscopy of Sections

Each of the specimen sections was removed from its mount and placed in the scanning electron microscope for observation. Micrographs were taken of both typical and unusual features and some nondispersive X-ray analyses were performed.

C. UNIVERSITY OF CONNECTICUT

Among the non-destructive evaluation methods, the measurement of sphericity presented some difficulty because of the intricate shape of some specimens that was difficult to define. The density measurement presented some difficulty because of liquid penetration inside cavities outcropping on the surface; these cavities had to be sealed off.

Among the destructive evaluation methods, it appeared difficult to use the Quantimet 720 with precision, because sometimes the contrast between second phases and micropores was very similar. In the core of some specimens microporosity was so fine that only X-ray microradiography could be used. Again, the quantitative value of this method is doubtful, because of the small areas covered at high magnification. Meaningful definition of dimensions appeared difficult also in macropores because of their intricate shapes. Serious difficulty appeared in identifying nonmetallic inclusions and in evaluating their volume percent and average size. In the bulk of the material, inclusions are so fine and rare that individual identification on the basis of optical properties or extraction followed by electron microprobe analysis become a serious problem.

The small mass of material available made complete and rigorous chemical analysis difficult, if not impossible. The concentration of the major alloying element was determined by wet chemical analysis. Carbon was evaluated by conductometry. Gases were analyzed by vacuum fusion technique, inert fusion or vacuum distillation analysis, or even emission spectrography, depending on the expected content. All minor elements were determined by emission spectrography.

II. CHARACTERIZATION RESULTS

A. SPHERICITY

The sphericity of Specimens SL-1.10 and SL-1.11 was measured by the University of Connecticut both micrometrically and by means of shadowgraphs. The accuracy of the micrometric measurements is $\pm$ 0.005 cm. The maximum dimension of the specimen is defined in this report as the Z dimension. The minimum dimension is defined as the X dimension, and the dimension on an axis orthogonal to the plane defined by the Z and X dimensions is reported as the intermediate, or Y dimension. It should be noted that all dimensions reported by the University of Connecticut are the radius, or one-half the diametrical dimension.

The coordinate system adopted for Specimens SL-2.2 and SL-2.6 assumed the original sting axis as the Z dimension, and the X and Y dimensions as the major and minor dimensions in an approximate equatorial plane orthogonal to the Z axis. The X and Y dimensions were provided to Arthur D. Little, Inc., by MSFC for Specimen SL-2.6. Additional measurements were made by Arthur D. Little, Inc., for both Specimens SL-2.2 and SL-2.6, by the shadowgraph technique. For these samples, the figures reported are the full diametrical dimension. The Z dimension does not include sting projections.

Specimen SL-1.9

No measurements were reported.

Specimen SL-1.10

X - 0.320 cm (micrometric), 0.343 cm (shadowgraph)
Y - 0.285 cm (micrometric), 0.293 cm (shadowgraph)
Z - 0.310 cm (micrometric), 0.327 cm (shadowgraph)

Specimen SL-1.11

Only a small fraction of the specimen melted and resolidified. It was, therefore, judged unimportant to make any measurements of sphericity.

Specimen SL-1.11

The local variation in surface topography as viewed in the shadowgraphs is approximately 0.005 cm. Measurements were made on the topographical peaks:

X - 0.66 cm
Y - 0.62 cm
Z - 0.67 cm

Specimen SL-2.5

Only a small fraction of the specimen melted and resolidified. It was, therefore, judged unimportant to make any measurements of sphericity.

Specimen SL-2.6

X - 0.236 inch (MSFC), 0.600 cm (0.236 inch)(shadowgraph)
Y - 0.232 inch (MSFC), 0.594 cm (0.234 inch)(shadowgraph)

Dimensions of the specimen along the Z axis were not judged meaningful because of a protuberance at the original sting location, variations of the surface near this protuberance, and the presence of another protuberance in the form of a cap region at the end opposite the sting.

B. STRUCTURAL AND CHEMICAL RESULTS

Specimen SL-1.9

Specimen SL-1.9 is a pure nickel material which was purposely retained on its sting after melting. The specimen is egg shaped and glossy with smooth dendritic features on the surface. The area near the sting position is curved and appears to have melted, at least internally, but had retained some of the machine markings of the original specimen surface. At the top of the specimen, opposite the sting area, is a slight protrusion. In and around this protrusion is a much finer dendritic structure. Figure 1.9-1 is a profile view of this specimen showing a small portion of the sting on the right and the protrusion previously mentioned on the left.

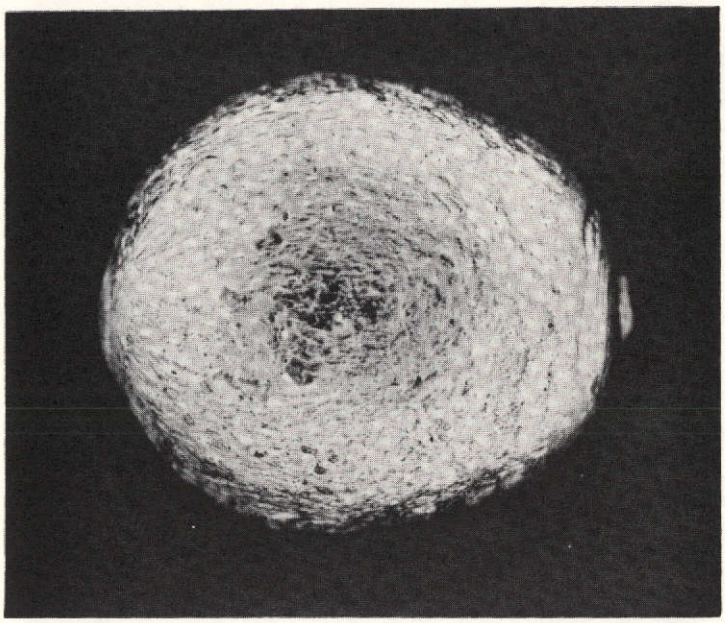

Figure 1.9-1 Photomacrograph of Specimen SL-1.9. Sting on the Right 10X (Georgia Institute of Technology)

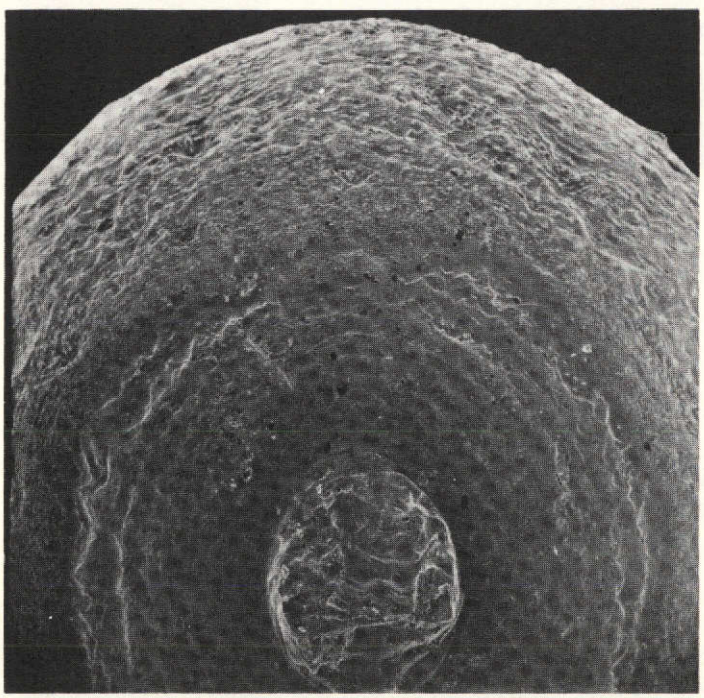

Figure 1.9-2 Scanning Electron Micrograph of Bottom or Sting End of Specimen SL-1.9. 25X (Georgia Institute of Technology)

Figure 1.9-2 is a low magnification scanning electron micrograph taken normal to the bottom or sting side of the sample. Some machine markings are seen close around the sting and ripple marking due to sample oscillation during solidification seen further away. A profile view of this area is shown in Figure 1.9-3. In this figure there appear two rings around the bottom of the specimen where the surface features change. Figure 1.9-4 is a higher magnification micrograph of the area of the ring closest to the sting. The ring further away is shown higher magnification in Figure 1.9-5. The surface features shown in the lower half of Figure 1.9-5 are representative of the surface from this second ring to about half way up the sample. The surface features nearer the top of the specimen are shown in Figure 1.9-6. The protrusion on the top of the specimen and the finer dendritic structure associated with it are shown in Figures 1.9-7 and 1.9-8.

Figure 1.9-9 is a macrograph of the polished and etched section of Specimen SL-1.9. The sting area is to the right. The etch-pit type of attack reveals columnar growth, originating at the sting area, and degenerating to a more random equiaxed dendrite-like structure at the opposite end of the specimen. The structure is shown at higher magnification in Figure 1.9-10.

Some contaminants were found uniformly distributed over the surface of the sample. Energy dispersive X-ray analysis of these contaminants gave varying amounts of the following elements: Al, Si, S, Cl, K, Ca and Ag. One particle found imbedded in a void gave high counts of Cr, Mn and Fe.

Emission spectrographic analysis of some of the material from the center of the specimen gave the following trace elemental content:

Si	20 ppm
Fe	5 ppm
Al	10 ppm
Cr	10 ppm

Electron microprobe analysis of the polished cross section revealed a small amount of oxygen in a few spots. No other elements were found. In general, the impurity content of the bulk sample is higher but not significantly so than the starting material, Table I.

Specimen SL-1.10

Features attributed to outcropping macroporosity are illustrated in the optical macrograph, Figure 1.10-1. At higher magnifications in the

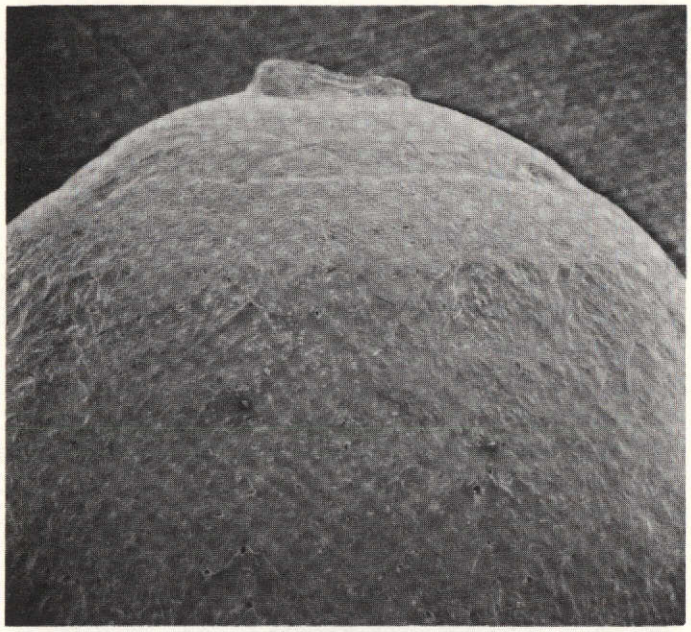

Figure 1.9-3 Scanning Electron Micrograph of Specimen SL-1.9, Profile View of Sting and Bottom of Sample 25X (Georgia Institute of Technology)

Figure 1.9-4 Scanning Electron Micrograph of Ring Nearest the Sting 250X

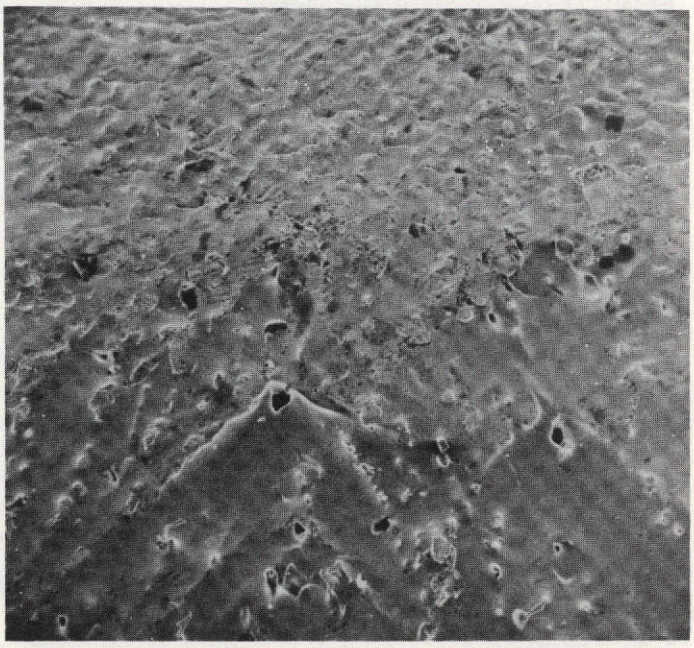

Figure 1.9-5 Scanning Electron Micrograph of Second Ring Near Sting 100X
(Georgia Institute of Technology)

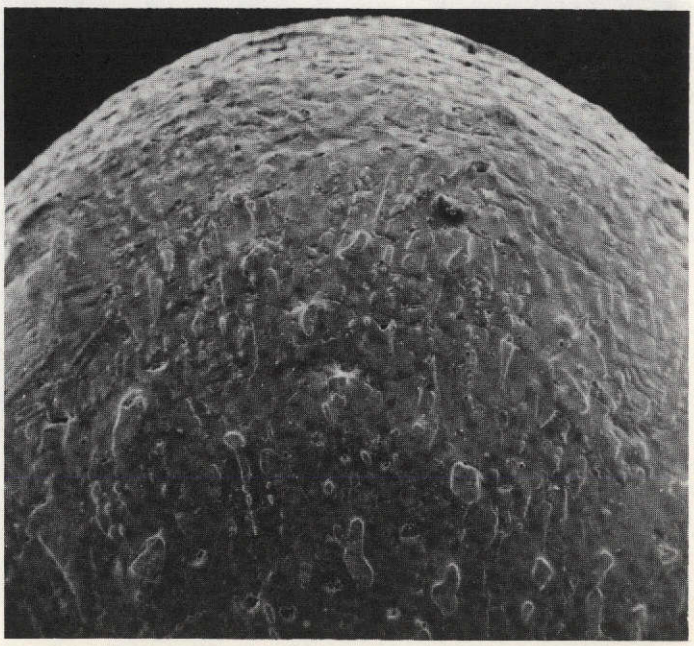

Figure 1.9-6 Surface Features of Specimen SL-1.9 Nearer to End Opposite Sting 25X
(Georiga Institute of Technology)

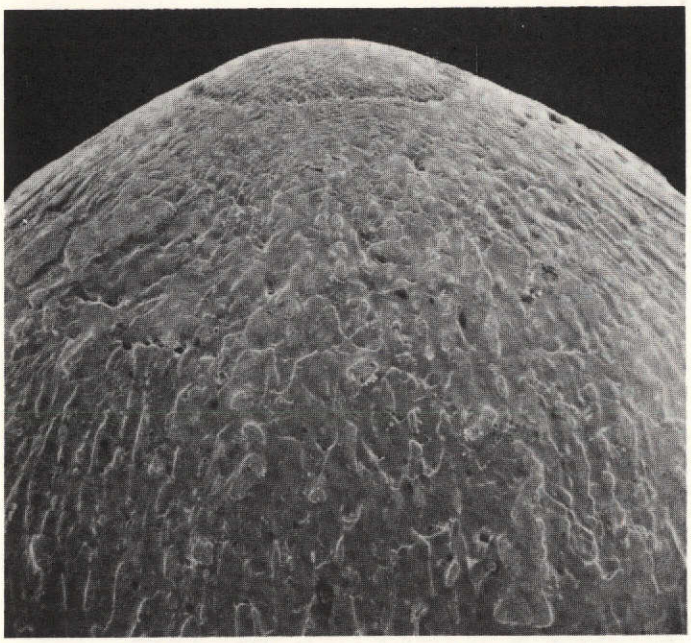

Figure 1.9-7 Scanning Electron Micrograph of Protrusion Opposite Sting End of Specimen SL-1.9 25X (Georgia Institute of Technology)

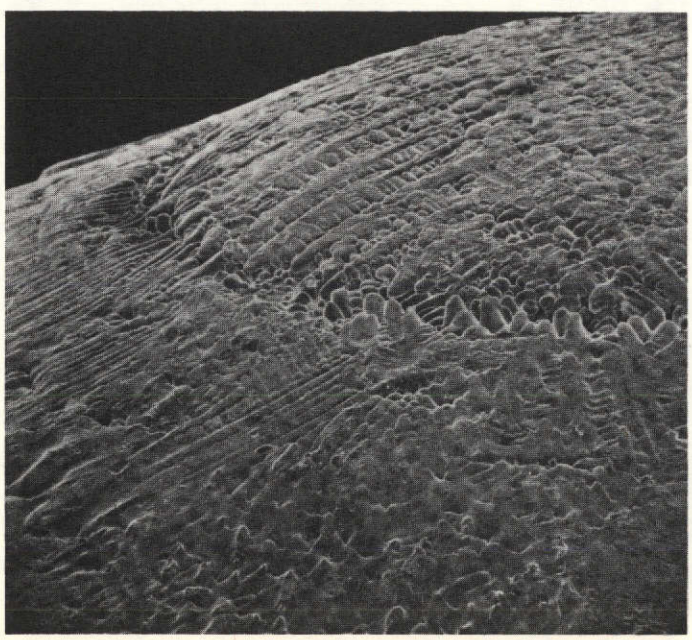

Figure 1.9-8 Scanning Electron Micrograph of Interface Area at Protrusion of Specimen SL-1.9 100X (Georgia Institute of Technology)

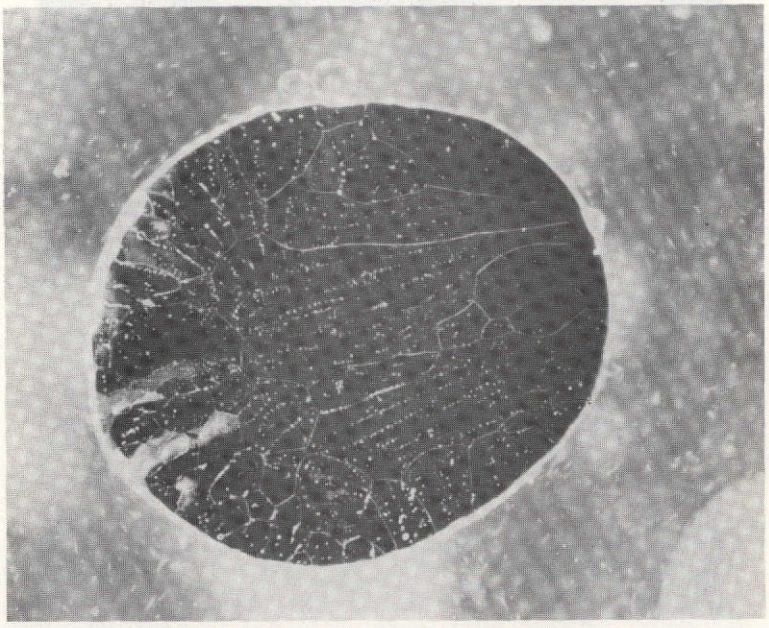

Figure 1.9-9 Macrograph of Cross Section of Specimen SL-1.9 10X
(Georgia Institute of Technology)

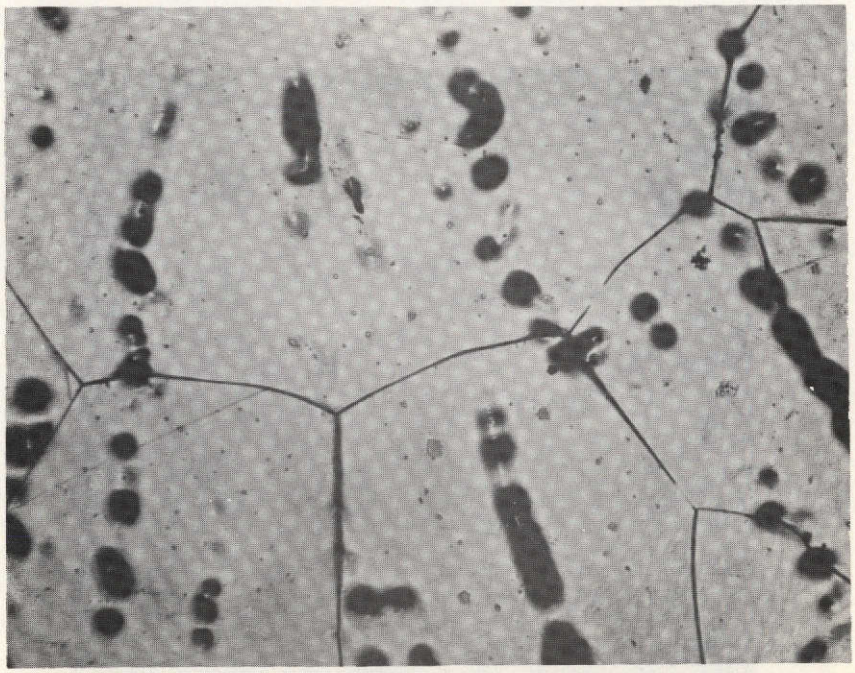

Figure 1.9-10 Higher Magnification Photomicrograph of
Cross Section of Specimen SL-1.9 100X
(Georgia Institute of Technology)

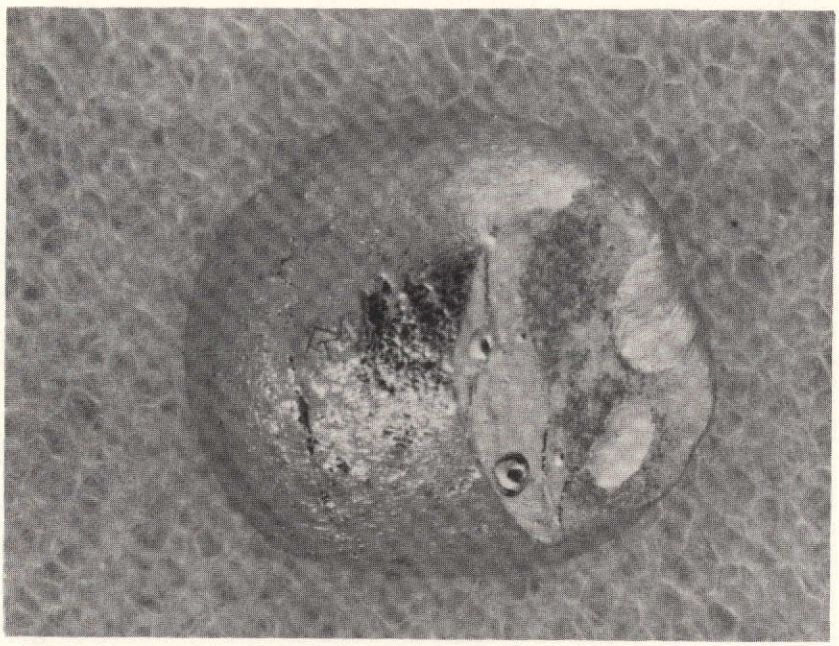

Figure 1.10-1 Photomacrograph of Specimen SL-1.10.
Sting on the Right 10X
(Marshall Space Flight Center)

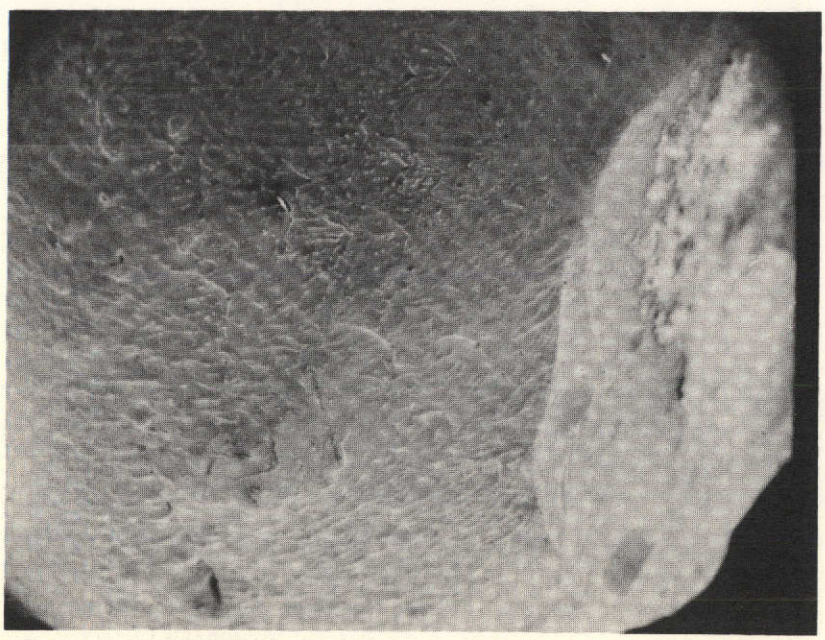

Figure 1.10-2 Scanning Electron Macrograph of Specimen SL-1.10.
Sting on Right 25X
(Marshall Space Flight Center)

scanning electron microscope surface patterns can be seen which are probably the result of fluid flow and vaporization during solidification, Figures 1.10-2, 1.10-3 and 1.10-4.

Metallographic cross section revealed two areas--one opposite the sting end of the sample that did not melt having an average grain size of 100μm and one at the sting end which did melt and in which the average grain size is 1000μm. No definite dendritic structure was observed in the melted and resolidified portion of the specimen. When heavily etched and examined under polarized light, a regular dendrite-like segregation pattern could be observed which may be attributed to impurity segregation, Figures 1.10-5 and 1.10-6. However, such impurities are extremely limited in light of the results of the bulk chemistry described below.

No secondary phases, microsegregation or macrosegregation were definitively detected or measured in this specimen. Some silica, silico-aluminate and sulfide inclusions were identified without certainty because of their extreme fineness.

While some microporosity is observed on the surface, Figure 1.10-1, almost no porosity is observed within the specimen. Quantitative metallographic and X-ray microradiographic analysis gave a volume percent of about 1.75%.

Chemical analysis revealed the following impurities; O:10ppm, N:5ppm, H:2ppm, Fe:4ppm, Cr:5ppm, Co:5ppm, Si:5ppm, Cu:10ppm. Referring to Table I, no significant changes in the chemistry were revealed.

The average microhardness was found to be equal to 155 VHN, both in the bulk of the grains and in the grain boundaries.

Specimen SL-1.11

Only a small fraction of the sample melted and resolidified, Figures 1.11-1 and 1.11-2. The surface morphology is illustrated by the scanning electron micrographs in Figures 1.11-3 and 1.11-4. There is no evidence of extensive porosity. Locally, in a shallow shrinkage cavity there is evidence of surface dendritic growth, Figure 1.11-4. The pattern shown in Figure 1.11-3 appears to be an ensemble of ripple-marks caused by limited displacement of partially melted or mushy metal. This displacement appears to have been guided by the machining marks on the underlying unmelted portion of the sample.

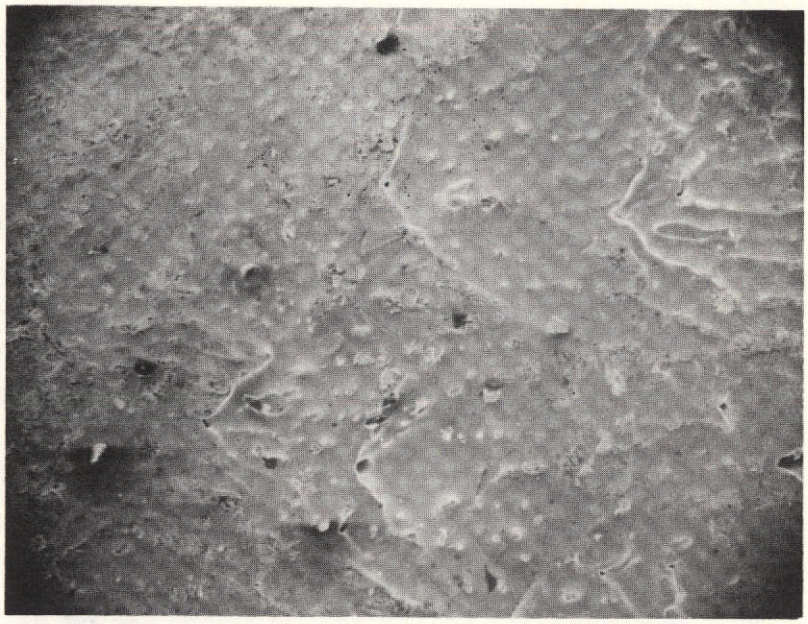

Figure 1.10-3 Scanning Electron Micrograph of Side of Specimen SL-1.10 100X
(Marshall Space Flight Center)

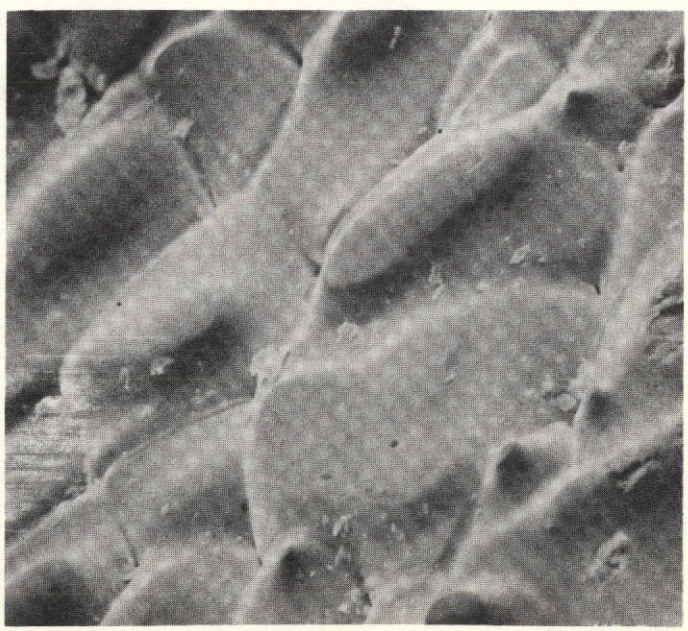

Figure 1.10-4 Scanning Electron Micrograph of Side of Specimen SL-1.10 600X
(University of Connecticut)

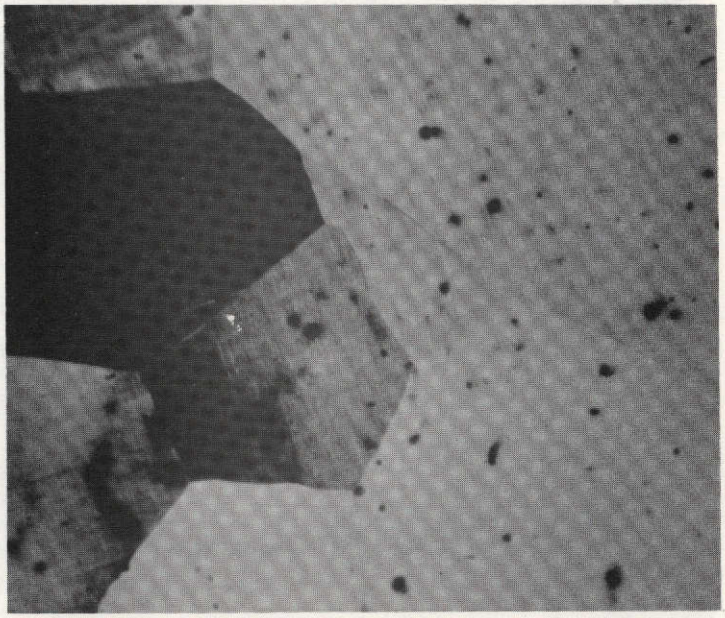

Figure 1.10-5 Polished and Etched Section of Specimen SL 1.10-Polarized Light 50X (University of Connecticut)

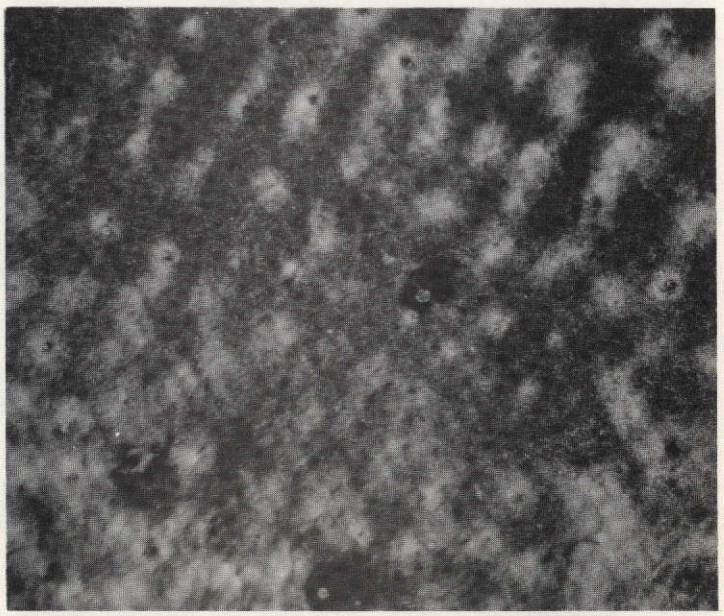

Figure 1.10-6 Polished and Etched Section of Specimen SL-1.10-Polarized Light 100X (University of Connecticut)

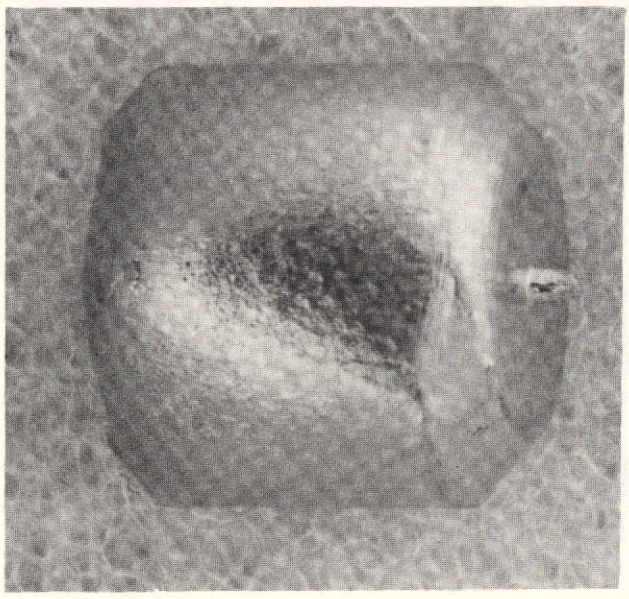

Figure 1.11-1 Photomacrograph of Specimen 1.11. Sting on Right 10X
(Marshall Space Flight Center)

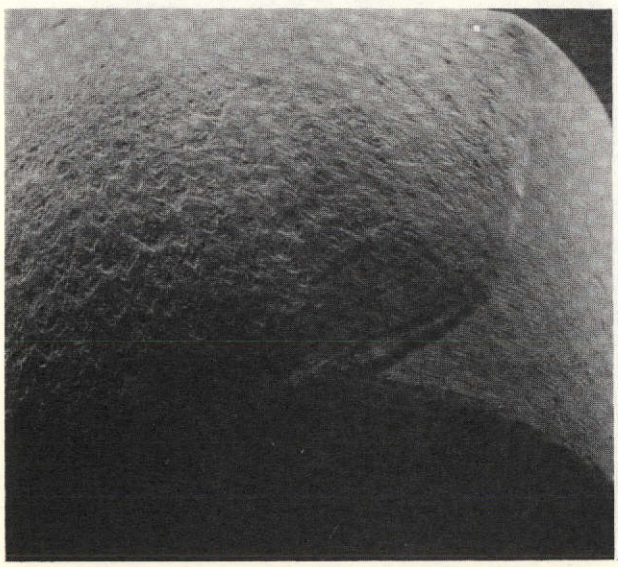

Figure 1.11-2 Scanning Electron Macrograph of Specimen SL-1.11 25X
(University of Connecticut)

Figure 1.11-3 Scanning Electron Micrograph of Surface of Specimen SL-1.11 100X
(University of Connecticut)

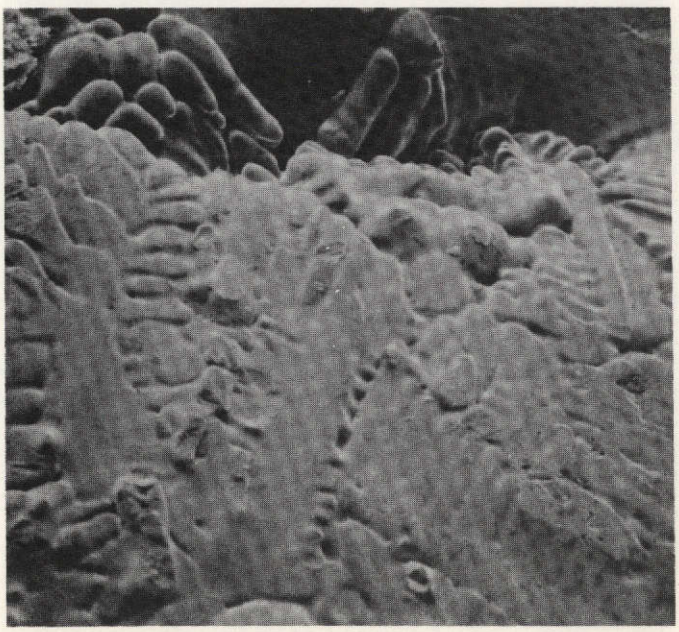

Figure 1.11-4 Scanning Electron Micrograph of Surface Shrinkage Cavity - Specimen SL-1.11 500X
(University of Connecticut)

The metallographic cross section of the sample exhibits the unmelted microstructure, Figure 1.11-5 and the melted portion, Figure 1.11-6, that resulted from solidification. The unmelted structure consists of heavily twinned grains of average grain size of 115 μm. The solidified structure consists of coarse equiaxial grains of average grain size 327 μm.

The dendrite structure that appeared in certain locations, Figure 1.11-4, did not appear in the bulk specimen. However, very heavy etching and examination in polarized light revealed a very vaguely dendrite-like segregation pattern, Figure 1.11-7. The surface dendrites are very fine, with a secondary arm spacing of about 5 μm.

No secondary phase, microsegregation or macrosegregation was observed. The non-metallic inclusions were similar to those observed in Specimen SL-1.10.

An average microhardness of about 150 VHN was found in the grain and at the grain boundaries.

The concentration of analyzed elements are: Cu:3ppm, Si:5ppm, Cr:5ppm, Fe:5ppm, Co:3ppm, O:15ppm, N:3ppm, and H:2ppm.

Specimen SL-2.2

Figures 2.2-1, 2.2-2 and 2.2-3 illustrate the surface topography of the specimen. The relatively coarse surface solidification of the retained nickel specimen, SL-2.2 is evident. File marks can be seen on the sting on this specimen. These were placed there during removal of the sample from the wheel and are oriented toward the electron beam. There is extensive surface solidification shrinkage, proceeding from a fine scale to a gross scale from the sting along the sides of the specimen. The top of the specimen is relatively shrinkage-free. There is a very slight evidence of a coarsened dendrite morphology in the surface islands, Figure 2.2-3. Solidification initiated at the sting and proceeded in a columnar manner in a family of cones about the Z axis. Near the top of the specimen, the solidification degenerates into a more random equiaxed type of structure.

The pitting-etch reveals a dendrite-like structure. This may be the result of impurity segregation, although the etchant (Carapella's reagent) produces effects quite different from those observed for Specimens SL-1.10 and SL-1.11 which were etched in Rosenhain's reagent.

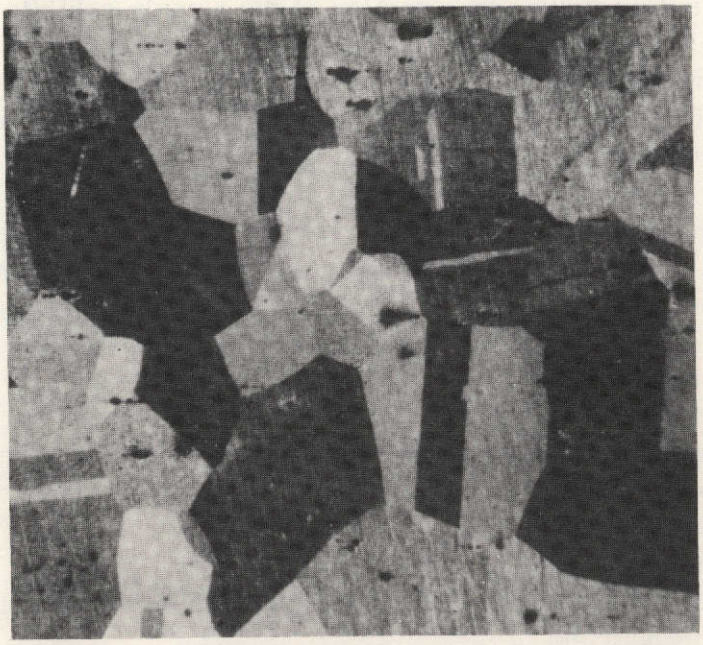

Figure 1.11-5 Cross Section of Specimen SL-1.11
Unmelted Area 50X
(University of Connecticut)

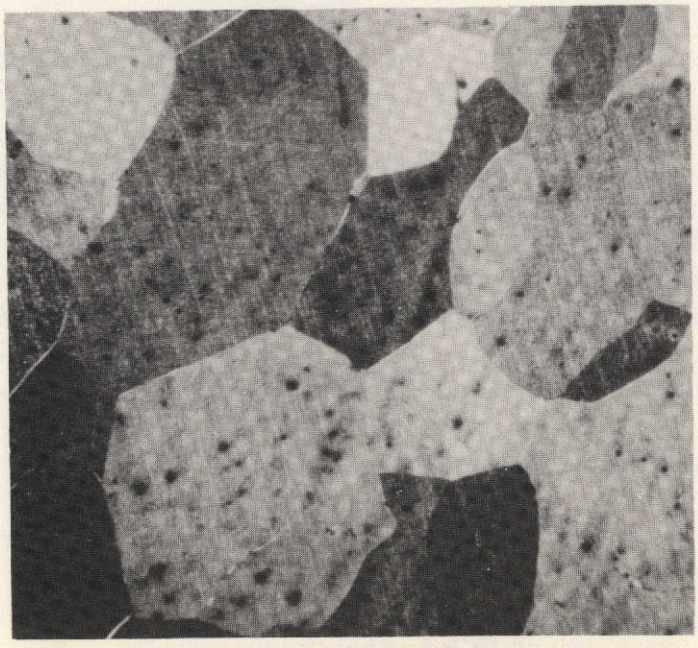

Figure 1.11-6 Cross Section of Specimen SL-1.11
Melted Area 50X
(University of Connecticut)

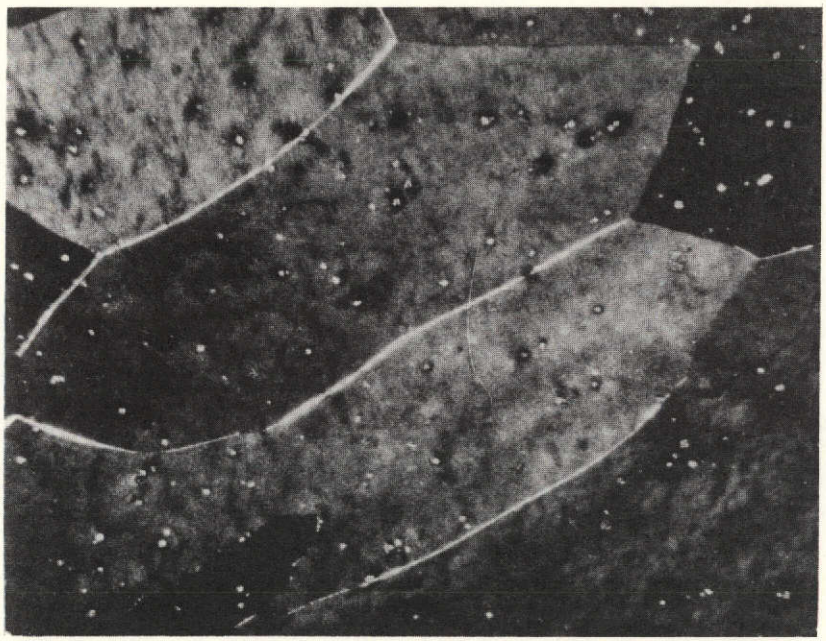

Figure 1.11-7 Cross Section of Specimen SL-1.11 100X
(University of Connecticut)

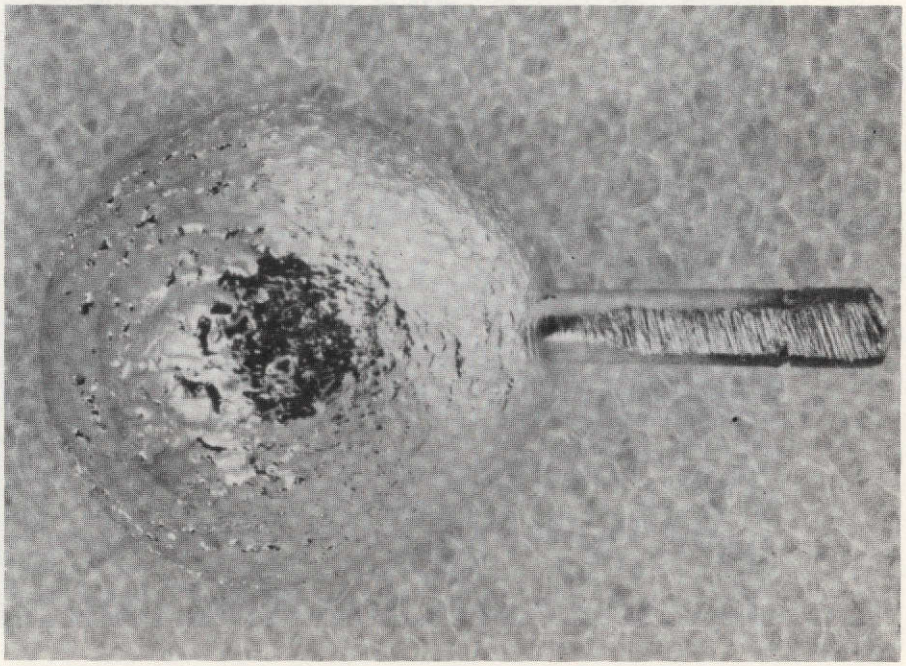

Figure 2.2-1 Photomacrograph of Specimen SL-2.2 10X
(Marshall Space Flight Center)

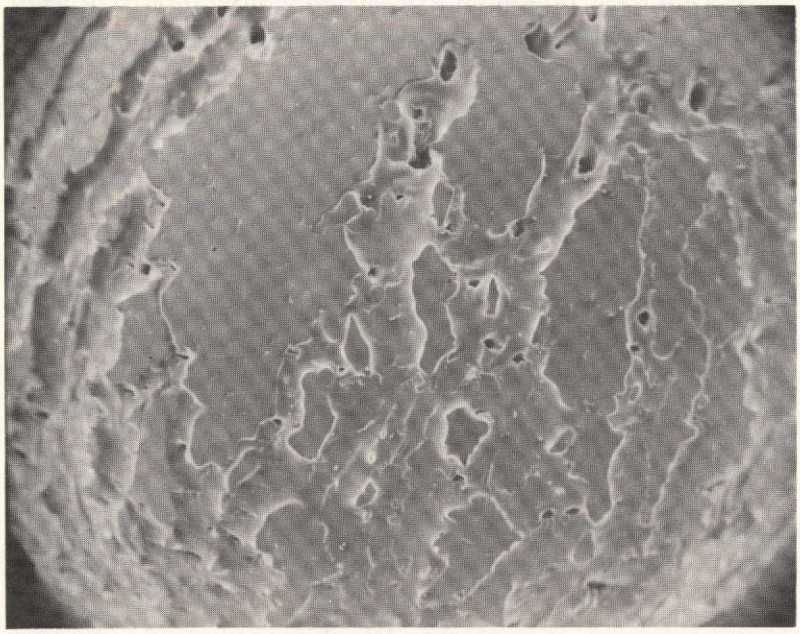

Figure 2.2-2 Scanning Electron Macrograph of Specimen SL-2.2 25X
(Marshall Space Flight Center

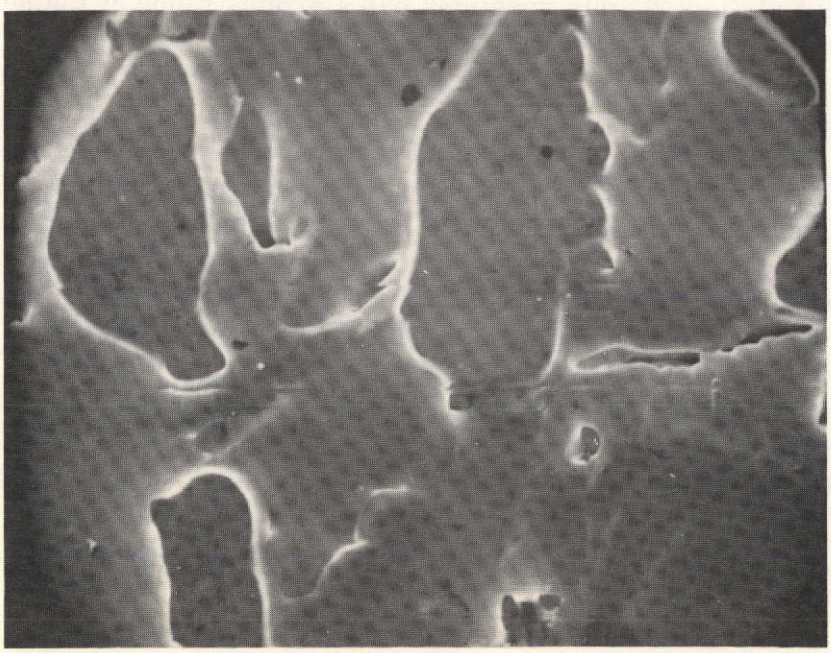

Figure 2.2-3 Scanning Electron Micrograph of Specimen SL-2.2 100X
(Arthur D. Little, Inc.)

In the columnar region, the average pit spacing is 50μ m, and can probably be interpreted as a measure of the secondary dendrite arm spacing, Figure 2.2-7. The average grain size of the sample is 600μ m.

The sting in a region near its point of attachment reveals a lack of melting with large grains, annealing twins, and a banded structure as a result of etch pitting, Figure 2.2-8.

A pinhole Laue X-ray diffraction from the top of the sample (opposite) the sting indicates that the beam was striking a single grain with the (001) orientation. Analysis on the side of the sample reveals a spotty pattern, indicating a large grain size but the beam is impinging on several grains. There is no spot fragmentation, indicating that little surface stress is present.

The hardness of the specimen averages 75 VHN, both in the grains and in the grain boundaries. The hardness of the sting at its extremity averages 130 VHN. All measurements were made using a load of 500 grams.

Specimen SL-2.5

No discussions of the results of Specimen SL-2.5 were provided for the purpose of this report with the exception of some photographs without commentary. However, several of these are included here because, like Specimens SL-1.9 and SL-2.6, this specimen has a protuberance at the end opposite the sting.

Specimen SL-2.5 is a release specimen which was only partially melted, Figure 2.5-1. The internal solidification pattern as revealed by the etched cross section is similar to the other pure nickel specimens, Figure 2.5-2. There is columnar growth in a direction away from the unmelted portion of the specimen (where annealing twins are very evident) and from the bottom or sting area in that region. Near the top of the specimen, the internal structure degenerates to a random, equiaxed, dendrite-like structure.

The protuberance at the top is shown in Figure 2.5-3 and 2.5-4. Although it is difficult to resolve, the structure in the protuberance appears to be two-dimensional dendritic, more like Specimen SL-1.9 than Specimen SL-2.6.

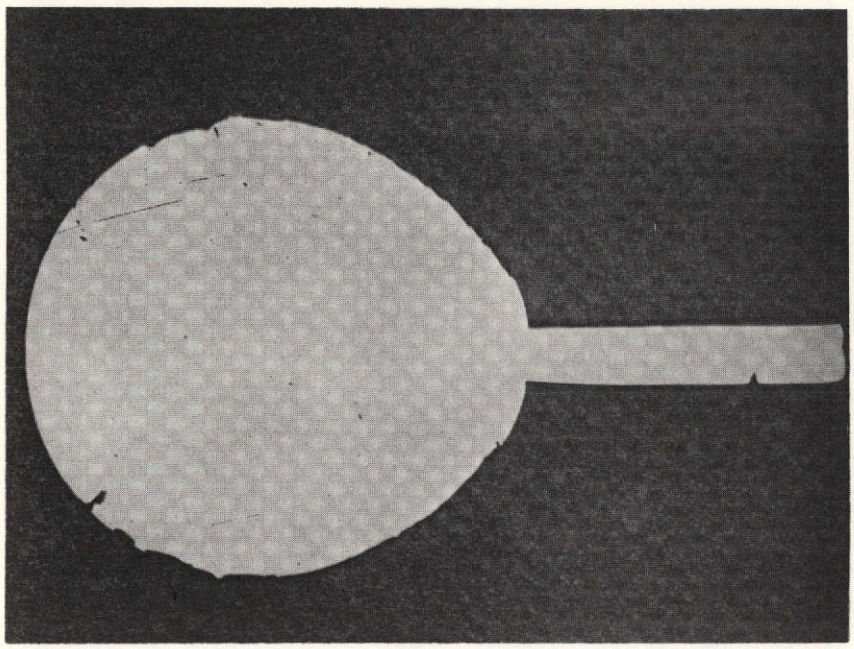

Figure 2.2-4 Unetched Cross Section of Specimen SL-2.2
(Arthur D. Little, Inc.) 10X

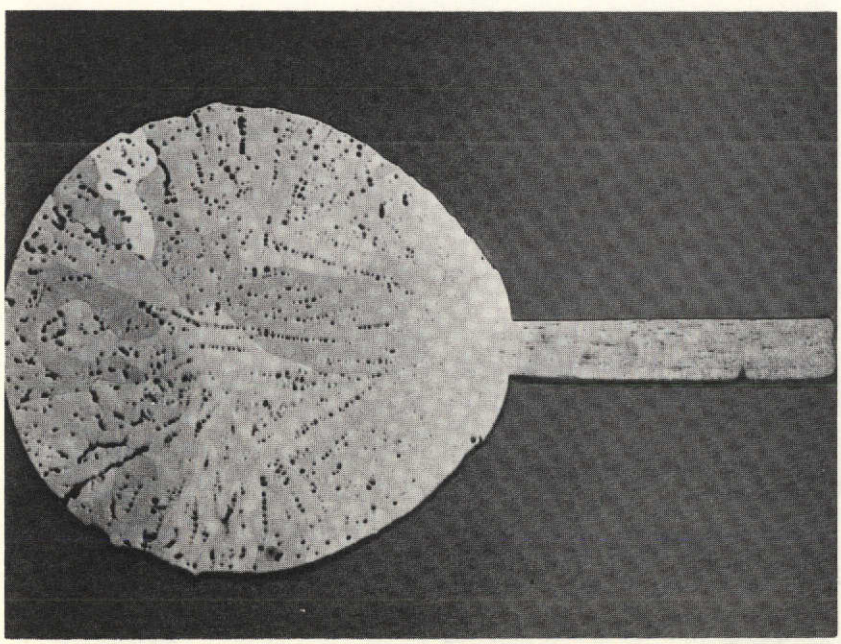

Figure 2.2-5 Etched Cross Section of Specimen SL-2.2
(Arthur D. Little, Inc.)

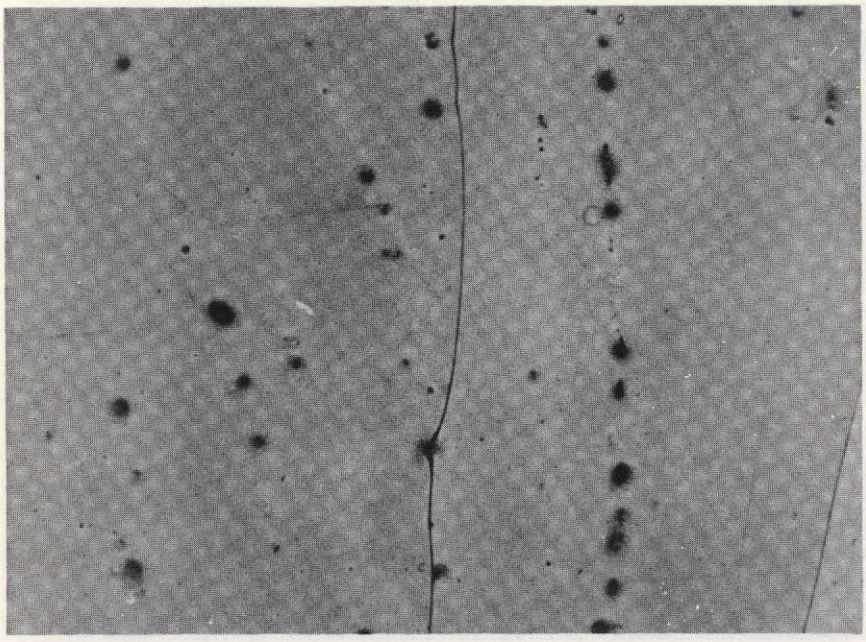

Figure 2.2-7 Etched Cross Section of Specimen SL-2.2
Columnar Zone 100X
(Arthur D. Little, Inc.)

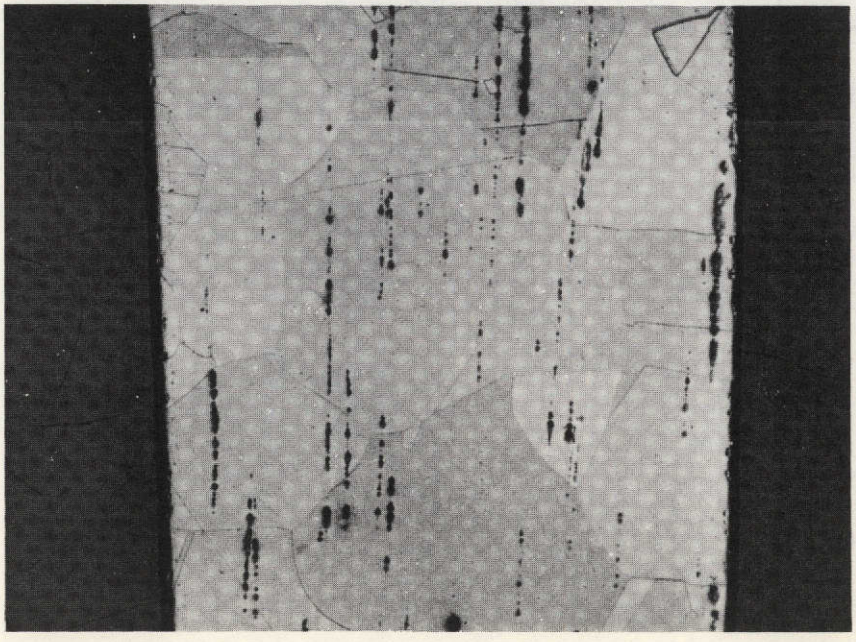

Figure 2.2-8 Etched Cross Section of Sting Near
Body of Specimen SL-2.2 100X
(Arthur D. Little, Inc.)

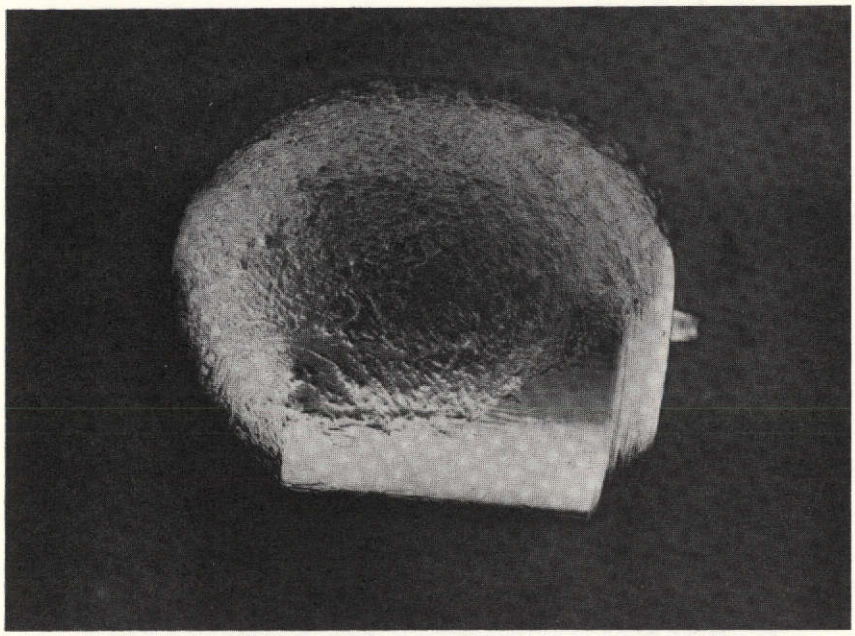

Figure 2.5-1 Photomacrograph of Specimen SL-2.5 10X
(Georgia Institute of Technology)

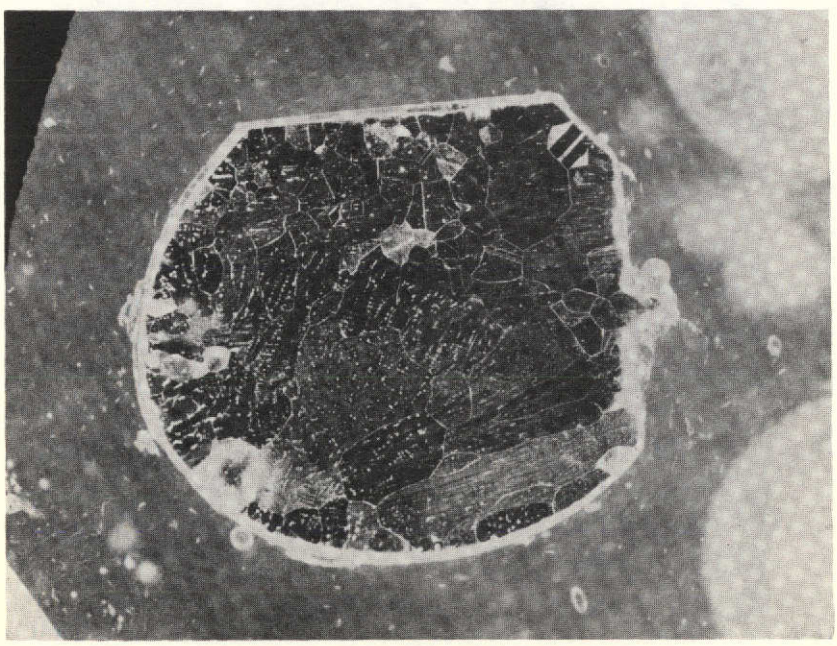

Figure 2.5-2 Polished and Etched Cross Section of Specimen SL-2.5 10X
(Georgia Institute of Technology)

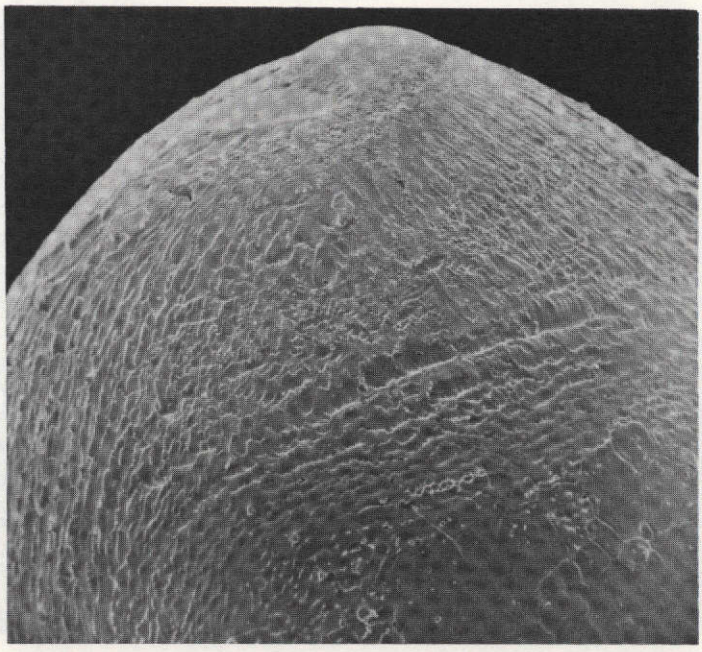

Figure 2.5-3 Scanning Electron Macrograph Showing Top Protuberance 25X
(Georgia Institute of Technology)

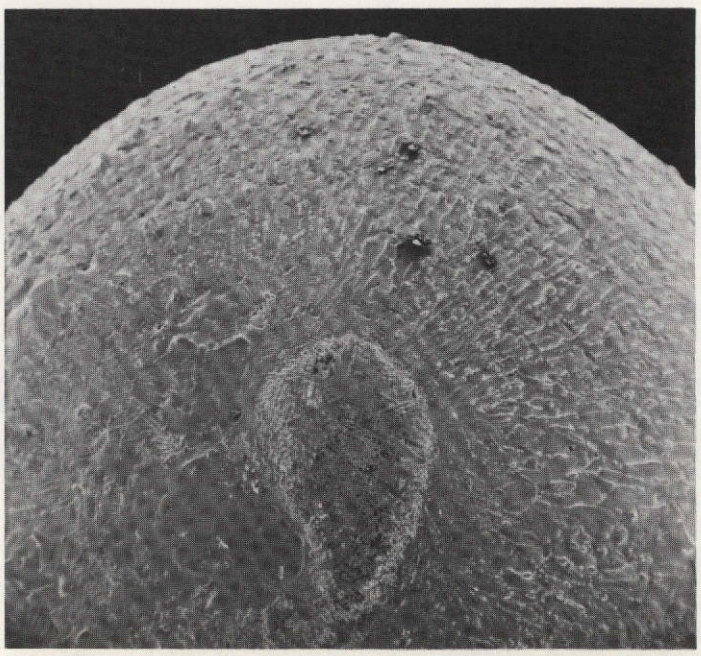

Figure 2.5-4 Scanning Electron Macrograph on End of Specimen SL-2.5 Opposite Sting 25X
(Georgia Institute of Technology)

Specimen SL-2.6

There are two features that are noteworthy about Specimen SL-2.6, Figure 2.6-1. Like Specimen SL-1.9 and SL-2.5, there is a cap or protuberance at the end of the specimen opposite the position of the original sting. Secondly, there is a protuberance at the position of the original sting. Its diameter matches that of the hole drilled in the ceramic pedestal more closely that it does the original diameters of either the captive or release stings.

The surface structure of the major portion of the specimen is similar to that for the other nickel specimens which had a significant fraction melted, with the exception of the captive Specimen SL-2.2, which had a much coarser structure, Figures 2.6-2, 2.6-3, compared to Figure 2.2-2. The surface patterns are also probably the result of fluid flow and vaporization during solidification. Specimen SL-2.6, however, has a cylindrical protuberance at the position of the sting which has a diameter of about 1.5 mm (.06 inch) as measured by the shadowgraph. It is apparent that either highly plastic or molten metal was drawn down into the hole in the pedestal before release of the sample. The projection did not subsequently have time to conform to the generally quite spherical contours of the remainder of the sample. Because of etching problems with pure nickel, it is not apparent whether this projection was molten or merely extremely plastic.

Specimen SL-2.6 also exhibits a fine grain region or cap at the pole of the Z-axis opposite the sting, Figures 2.6-4, 2.6-5 and 2.6-6. The diameter of the cap is approximately .075 cm (0.03 inch) and protrudes at its center about 0.018 cm (.007 inch) above an arc fitted to the curvature of the rest of the top of the sample. The grains in this cap are equiaxed, approximately 25 μm (.001 inch) in diameter. The cap probably represents an area of independent nucleation events in which spherical nuclei did not have the opportunity to develop any discernible surface dendritic characteristics before impinging upon each other. It is believed that the structure results from fast thermal undercooling, although constitutional supercooling may have played a role even in the relatively pure nickel. It is not believed that homogeneous nucleation occurred. There are probably a sufficient number of nucleation embryos in the form of material impurities (inclusions and oxides) to account for the structure.

Internal porosity, as revealed by the unetched cross section, is very minimal, Figure 2.6-7. Except for the cap region, the internal solidification structure is similar to and can be explained in the same manner as the other nickel samples, Figure 2.6-8.

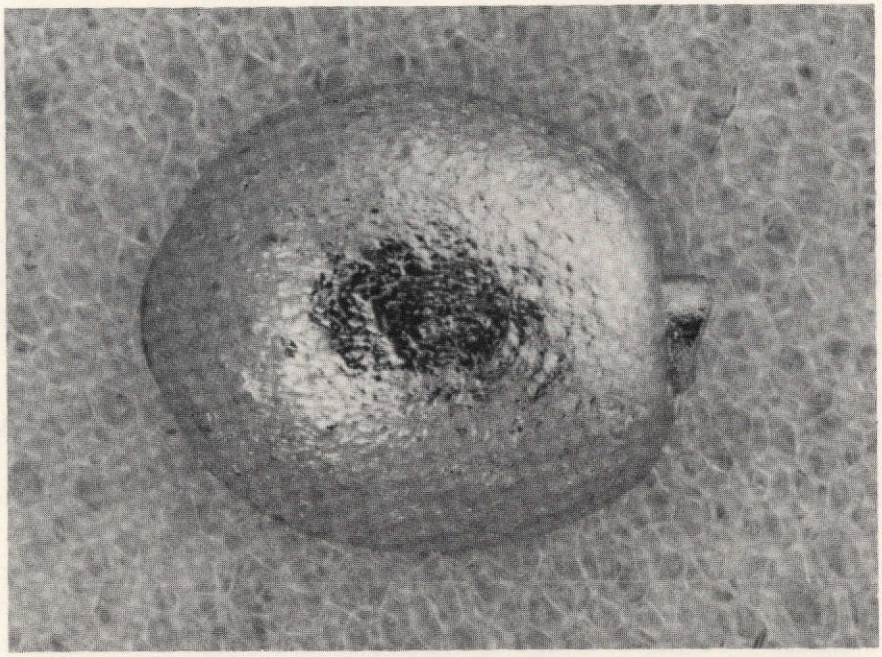

Figure 2.6-1 Photomacrograph of Specimen SL-2.6
(Marshall Space Flight Center) 10X

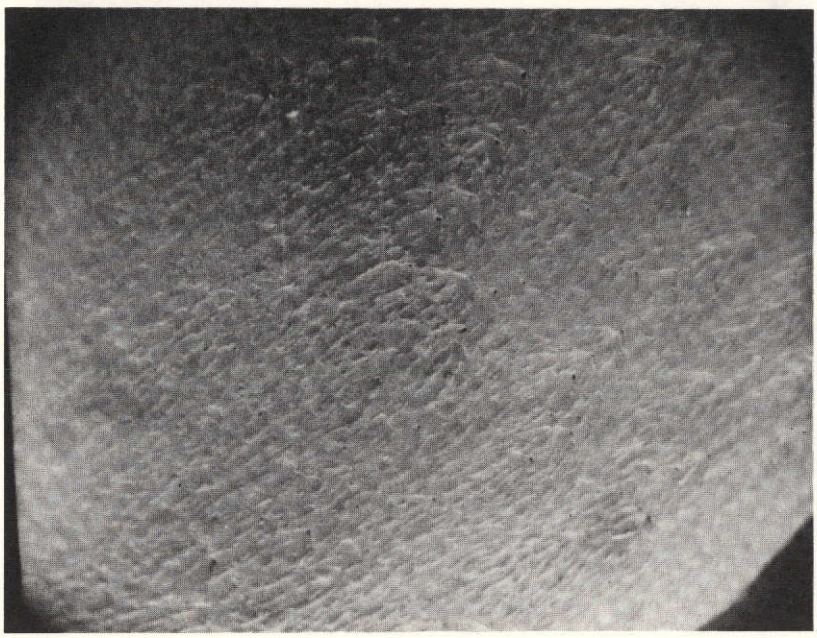

Figure 2.6-2 Scanning Electron Macrograph of Specimen SL-2.6 25X
(Marshall Space Flight Center)

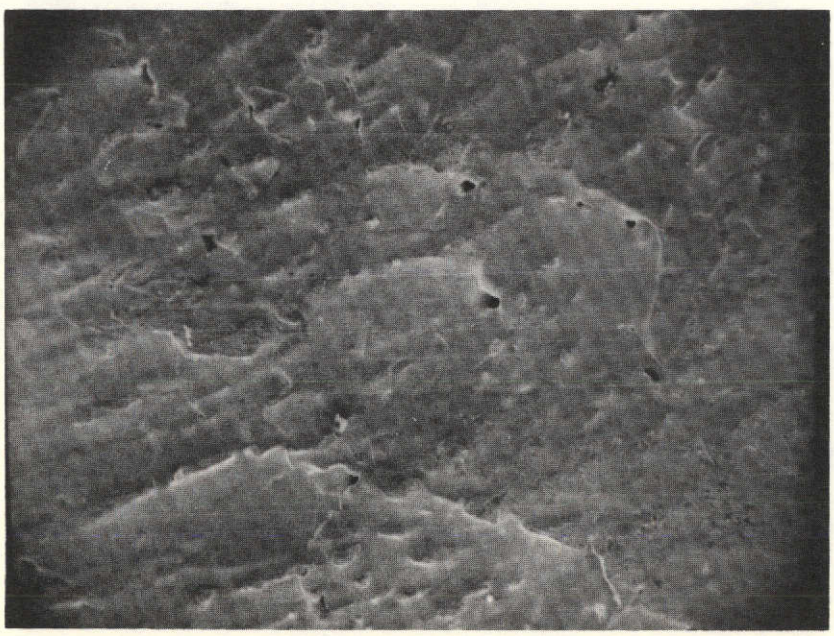

Figure 2.6-3 Scanning Electron Micrograph of Specimen SL-2.6
(Marhsall Space Flight Center)

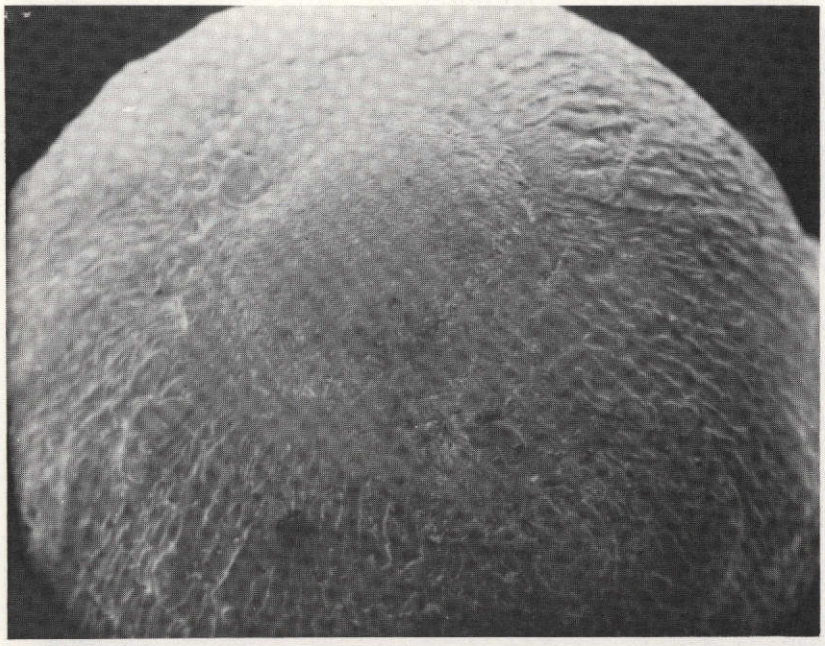

Figure 2.6-4 Scanning Electron Micrograph of Cap Region on Specimen SL-2.6 50X (Arthur D. Little, Inc.)

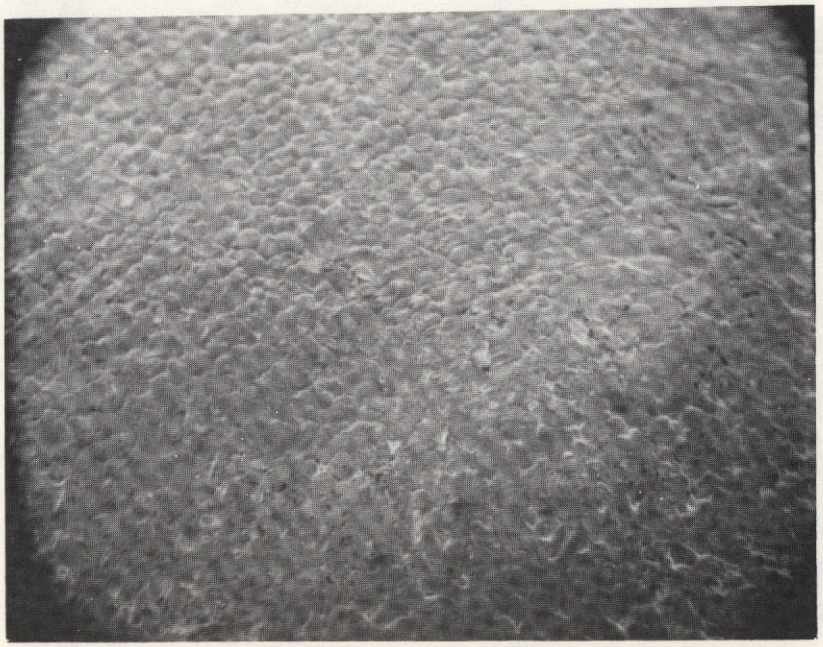

Figure 2.6-5 Scanning Electron Micrograph of Cap Region on Specimen SL-2.6 100X (Arthur D. Little, Inc.

Figure 2.6-6 Scanning Electron Micrograph of Cap Region on Specimen SL-2.6 600X (Arthur D. Little, Inc.)

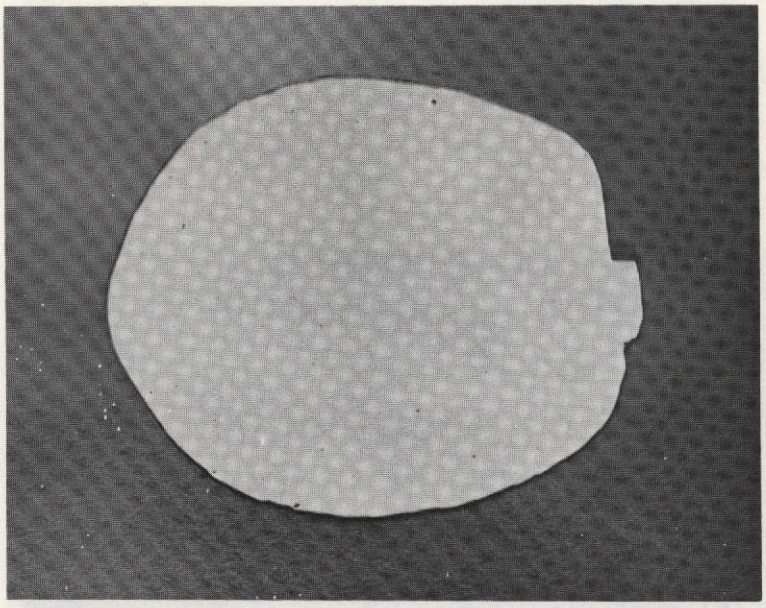

Figure 2.6-7 Unetched Cross Section of Specimen SL-2.6
(Arthur D. Little, Inc.) 10X

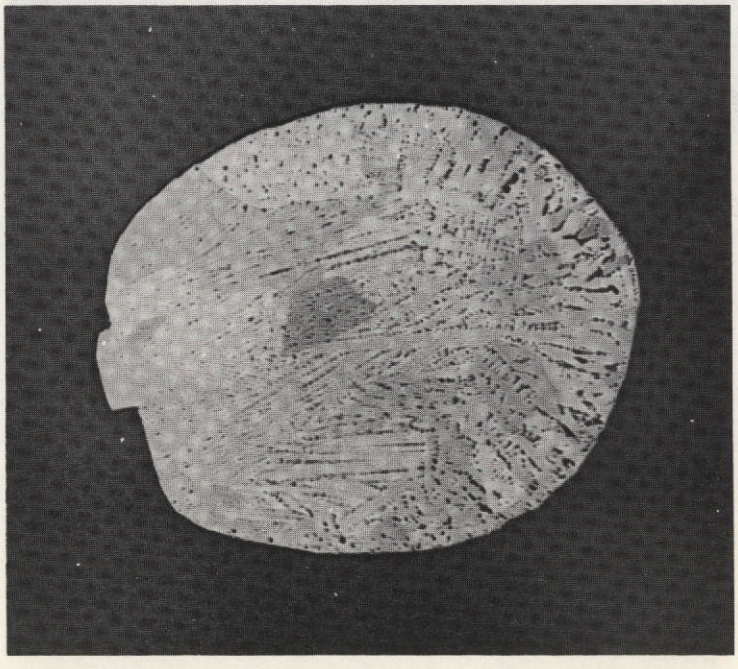

Figure 2.6-8 Etched Cross Section of Specimen SL-2.6
(Arthur D. Little, Inc.)

The etch pits in the columnar region of the specimen are spaced approximately 50 μm, Figure 2.6-9. The recrystallized grain structure is again quite large, 750 μm average. Due to etching difficulties, the structure in the cap region is not instructive, except that there appears to be chemical differences and a lack of subsurface shrinkage porosity usually associated with cap structures.

There is no difference between pinhole Laue X-ray diffraction patterns from the side and cap areas. Both are random spot patterns with superimposed arcs indicative of a thin, highly oriented polycrystalline surface layer in both regions. There is no evidence of surface strain.

The hardness of the specimen averages about 100 VHN, both in the grains and the grain boundaries. The hardness was measured with a load of 500 grams.

Both X-ray fluorescence analysis and energy dispersive X-ray analysis of the cap region failed to detect any elements other than nickel, although it must be recognized that these techniques are relatively insensitive to low impurity levels.

DISCUSSION

Specimen SL-1.9

The retained specimen melted almost completely, except in the area near the sting, where machining marks are still visible. The ring nearest the specimen is probably a region of partial melting. The second ring around the bottom of the specimen appears to represent an area in which solidification occurred fairly rapidly and reflects solidification under oscillating conditions which becomes less apparent as the solidification rate decreased and surface fluid flow and vaporization phenomena predominated to provide the surface morphology observed over the bulk of the specimen. Internally, solidification in the bulk of the specimen proceeded in a columnar manner away from the unmelted material at the bottom of the specimen and then converted to an equiaxed dendrite-like structure near the top of the sample. The large grain size is the result of subsequent recrystallization of the relatively pure nickel.

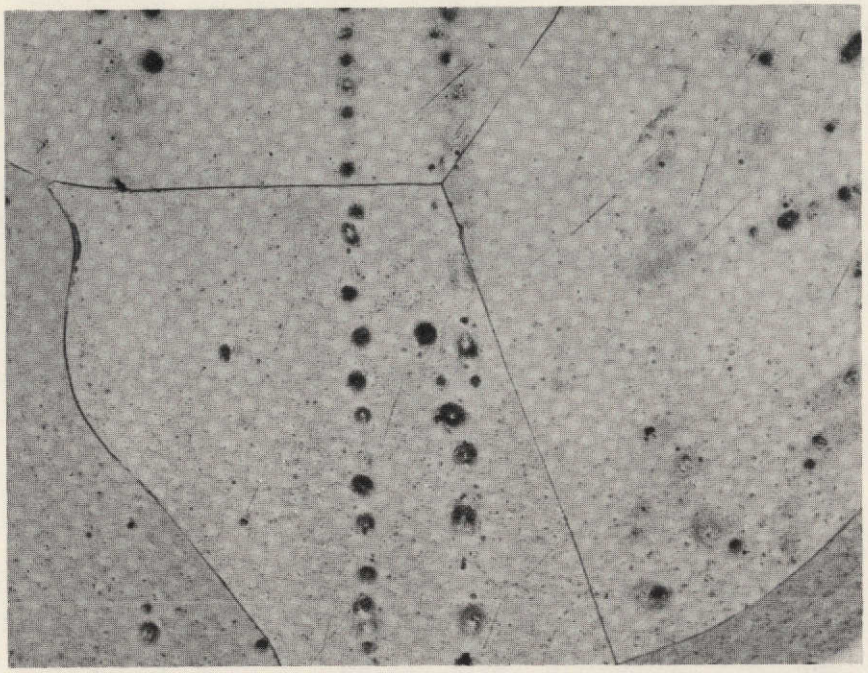

Figure 2.6-9 Cross Section of Specimen SL-2.6 in the Region of Columnar Growth 100X (Arthur D. Little, Inc.)

The end of the specimen near the sting exhibits a two-dimensional surface structure consisting of a region of independent surface nucleation and growth. The center of this contains equiaxed grains which nucleated, grew, and impinged upon each other before dendritic growth could develop. They are surrounded by a ring of extremely fine dendrites resulting from a sufficient impurity level buildup to allow such growth. This cap area, while representing a region of independent nucleation, does not imply homogenous nucleation, although some undercooling probably occurred in this very local region.

Specimen SL-1.10

The specimen melted partially and resolidified epitaxially on the remaining unmelted solid. Some typical shrinkage microporosity appears on the surface, especially at the boundary between resolidified and unmelted parts. Ripple marks appearing on the surface may be attributed to limited displacement of mushy liquid. Cellular patterns may be attributed to surface vaporization along boundaries of dendrite cells that might have grown at some locations of the surface. Extensive grain growth after completion of solidification, favored by the purity of the material, should be held responsible for the large grain size observed. The weak dendritic segregation pattern revealed by heavy etchings and examination of the specimen under polarized light may be attributed to impurities. The solidification of this specimen is similar to that of the ground pure nickel specimens, with the exception of the ripple marks that appear only in the Skylab specimen. There is no evidence of undercooling. There is no evidence of a cap or protuberance such as was observed on Specimens SL-1.9, SL-2.5 and SL-2.6.

Specimen SL-1.11

The microstructure and solidification behavior of this specimen is very similar to that of Specimen 1.10. Both melted partially and in both the solid grew epitaxially on the unmelted specimen. The observed weak dendritic segregation pattern exhibits equally fine spacing in both cases. The surface dendritic pattern observed in a shallow solidification cavity in this specimen may be attributed to impurity segregation or could be of thermal origin. Such patterns were observed in pure nickel ground specimens too. Ripple marks appearing on the surface may be attributed to limited displacement of mushy metal; this displacement appears to have been guided by the machining lines on the underlying unmelted specimen. Some of the surface relief could be attributed to impurity vaporization. The specimen did not undercool. There is no evidence of a cap or protuberance such as was observed on Specimens SL-1.9, SL-2.5 and SL-2.6.

Specimen SL-2.2

This retained nickel specimen, as was true of all of the specimens on wheel number 2, was heated for a relatively longer period of time than those on wheel number 1. For the nickel specimens, the chief implication is that the specimens were initially more uniform in temperature and the retained specimens were influenced by the proximity of a hotter sting material which may have slowed the solidification rate for Specimen SL-2.2. The slower solidification rate is believed to account for the relatively coarse surface structure of this specimen. In other respects, it is similar to the other pure nickel samples in terms of the internal columnar and equiaxed structures and the large recrystallized grain size. There was no undercooling and there is no evidence of a cap or protuberance of fine structure on the surface such as was observed for Specimens SL-1.9, SL-2.5 and SL-2.6.

Specimen SL-2.5

This specimen was only partially melted, and the columnar growth typical of the nickel specimens proceeded not only from the sting end of the specimen but from the unmelted portion of the specimen as well. Specimen SL-2.5 contains a small protuberance or area of independent two-dimensional surface growth as do SL-1.9 and SL-2.6. In this case, the fine grain area appears to consist almost entirely of fine grained dendrites. No impinged equiaxed grains can be observed.

Specimen SL-2.6

As with two of the other pure nickel samples, this specimen has a region of extremely fine, two-dimensional grain structure opposite the sting. Unlike SL-1.9, which appears to consist of a combination of fine equiaxed grains surrounded by a ring of dendrites, and SL-2.5 which appears to consist almost entirely of fine dendrites; the cap area on SL-2.6 consists almost entirely of fine 25 μm non-dendritic grains. In other respects, its structure is similar to the other nickel specimens.

DISCUSSION - SUMMARY

The only significant feature which was observed on the pure nickel flight specimens which differed significantly from the ground-based specimens is a region or cap of very fine two-dimensional surface growth structure at the top of the samples. This fine grain region was observed on three of the six samples evaluated. Such two-dimensional surface growth structures have been observed both on the ground-based specimens and on other surface areas of the flight specimens. However, the fine structures observed on the three flight samples are at least an order of magnitude finer than those previously observed, and resembly similar localized, fine, two-dimensional surface structures observed in both ground and flight specimens for the nickel alloys. The two-dimensional growth areas consist primarily of fine equiaxed grains in one specimen, SL-2.6, fine dendrites, SL-2.5, or a core of fine equiaxed grains surrounded by a ring of fine dendrites, Specimen SL-1.9.

A possible explanation for these structures is decreased bulk convection of the remnant liquid in the flight specimens as a result of the low gravity conditions. The flight specimen movie records show considerable turbulence or convection. It nevertheless may have been less than in the ground-based specimens. As the bulk of the specimens solidified, usually from the sting region and unmelted portions of the specimens, the latent heat of fusion released would not tend to distribute by means of bulk fluid flow as rapidly under conditions of relatively lower bulk fluid convection. This would tend to enhance the establishment of thermal conditions at the areas most remote from the advancing solid, such as the cap areas, which would favor independent two-dimensional nucleation and growth in these areas. There certainly are other factors involved, however, since not all of the pure nickel flight specimens exhibit this phenomenon. In the case of the slowly heated retained Specimen SL-2.2, this may be explained in terms of a relatively slow solidification rate. Thermal conduction of the latent heat through the remnant liquid would tend to negate favorable thermal conditions at areas remote from the growing solid even under conditions of minimized bulk fluid convection. The bulk of the specimens did not exhibit any solidification features which can be attributed to low gravity processing. There was no homogeneous nucleation or significant undercooling in the bulk. There may have been some slight undercooling in the areas of fine two-dimensional growth.

☆U.S. GOVERMENT PRINTING OFFICE 1974 – 640-446 / 107 REGION NO. 4